PHYSICAL REVIEW B **85**, 035210 (2012)

Implications of the formation of small polarons in Li_2O_2 for Li-air batteries

Joongoo Kang,[1,*] Yoon Seok Jung,[2] Su-Huai Wei,[1] and Anne C. Dillon[1]
[1]*National Renewable Energy Laboratory, Golden, Colorado 80401, USA*
[2]*Ulsan National Institute of Science and Technology (UNIST), Ulsan 689-798, Korea*
(Received 13 December 2011; published 23 January 2012)

Lithium–air batteries (LABs) are an intriguing next-generation technology due to their high theoretical energy density of ∼11 kWh/kg. However, LABs are hindered by both poor rate capability and significant polarization in cell voltage, primarily due to the formation of Li_2O_2 in the air cathode. Here, by employing hybrid density functional theory, we show that the formation of small polarons in Li_2O_2 limits electron transport. Consequently, the low electron mobility $\mu = 10^{-10}$–10^{-9} cm^2/V s contributes to both the poor rate capability and the polarization that limit the LAB power and energy densities. The self-trapping of electrons in the small polarons arises from the molecular nature of the conduction band states of Li_2O_2 and the strong spin polarization of the O $2p$ state. Our understanding of the polaronic electron transport in Li_2O_2 suggests that designing alternative carrier conduction paths for the cathode reaction could significantly improve the performance of LABs at high current densities.

DOI: 10.1103/PhysRevB.85.035210 PACS number(s): 82.47.Aa, 71.38.Ht, 72.20.−i

I. INTRODUCTION

Lithium–air batteries (LABs) have recently been revitalized as a promising electrical energy storage system due to their exceptionally high theoretical energy density.[1–8] LABs differ from conventional Li–ion batteries (LIBs) due to the reaction mechanism at the air cathode (AC). The most commonly employed LIB cathode is $LiCoO_2$, where Li deintercalation and intercalation occurs during charge and discharge, respectively. In contrast, O_2 molecules from the air react with Li^+ in the AC of LABs. Thus, during discharge, the O_2 molecules are reduced in the presence of Li^+ to primarily form lithium peroxide (Li_2O_2). The decomposition of the Li_2O_2 subsequently occurs upon charging. Theoretically, LABs may provide a high energy density of ∼11 kWh/kg compared to conventional LIBs (e.g., $LiCoO_2$/graphite), which have an energy density of only ∼0.4 kWh/kg (Ref. 4). The high energy density of LABs stems from the high capacity of Li metal (3862 mAh/g) and from the oxygen supply from air. However, including the weight of the electrolyte and AC, generally composed of porous carbon, the theoretical energy density becomes ∼2.8 kWh/kg (Ref. 8), still far exceeding the commonly employed $LiCoO_2$/graphite Li–ion technology.

Unfortunately, LABs suffer from poor rate capability and large hysteresis (or polarization) in the charge/discharge voltage profiles.[2–7] These challenges must be overcome prior to practical application of LABs. However, the fundamental origins that contribute to both of these issues are largely unclear. The polarization must be reduced to achieve high energy density and efficiency. This dictates that the Li_2O_2 at the oxygen cathode must have sufficiently high electronic conductivity. During discharge, the reaction that forms the Li_2O_2 is represented by $2Li^+ + 2e + O_2 \rightarrow Li_2O_2$. Also, a recent theoretical study[5] proposed a reaction mechanism in which the formation of Li_2O_2 is promoted on the surface of Li_2O_2 particles. High power density can only be achieved via rapid formation of Li_2O_2, dictating fast electron transfer from a substrate to the surface through the already-formed Li_2O_2 layers. Thus, fundamental understanding of the electron conduction mechanism in Li_2O_2 is crucial to improving the performance of the AC for LABs.

Unlike the case of free electrons in a rigid crystal, an electron's energy may be lowered by polarizing or deforming its surrounding lattice in such a way that the electron is localized by the distortion-induced attractive potential, i.e., forming a small polaron (see, e.g., Refs. 9–13 and references therein). Then, electron transport occurs via polaron hopping, which is usually described by the Marcus theory[14] and the Emin-Holstein theory.[15] Here, using first-principles calculations, we reveal that the self-trapping of electrons in small polaron states leads to extremely low electron mobility in Li_2O_2. The slow electron transfer via polaron hopping thus limits both power and energy densities of LABs. The finding of free, small polarons in a stochiometric, "transition-metal (TM)–free" Li_2O_2 is remarkable, considering that the formation of small polarons in oxides (e.g., $LiNbO_3$,[10,12] $LiFePO_4$,[11] $BaTiO_3$,[13] and ZnO:Li[16]) generally involves a change of the charge states of TM cations or O anions at defect sites. We present a novel, microscopic mechanism for the formation of small polarons in Li_2O_2, in which the molecular nature of the conduction band states and the strong spin polarization of the O $2p$ state lead to the self-trapping of an electron at a broken O–O site.

II. CALCULATION METHODS

In our study, the formation and migration of small polarons in bulk Li_2O_2 were calculated using a supercell with 192 atoms [Fig. 1(a)]. The primitive unit cell of Li_2O_2 has a hexagonal crystal structure (space group $P6_3/mmc$).[17,18] Total energies and electronic structures were calculated using the screened Heyd-Scuseria-Ernzerhof (HSE) hybrid density functional,[19] as implemented in the Vienna *ab initio* simulation package.[20] We found that results obtained using the Perdew-Burke-Ernzerhof generalized gradient approximation functional[21] are qualitatively similar. We used projector-augmented wave potentials[22] and a plane wave cutoff of 400 eV with k-point sampling of $2 \times 2 \times 1$ for the supercell calculations. The error in the formation energy of a small polaron due to k-point sampling is estimated to be less than 50 meV.

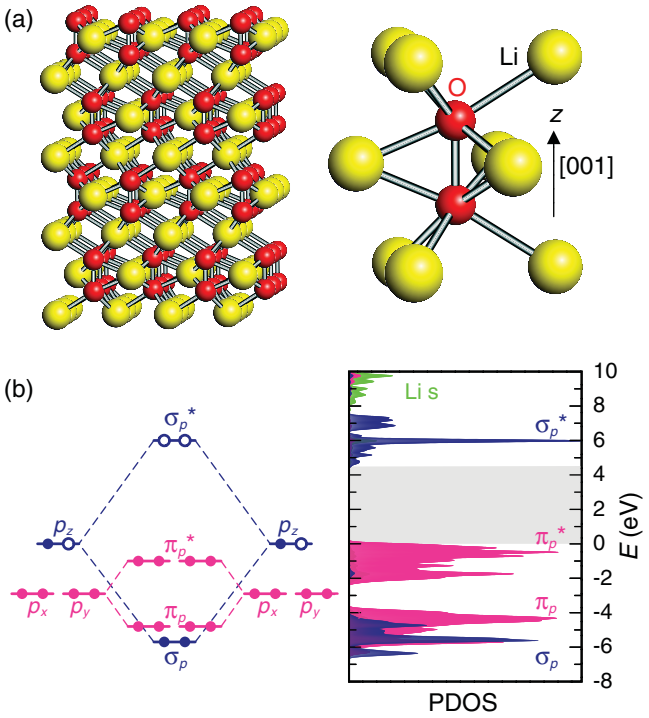

FIG. 1. (Color online) (a) A ball-and-stick model of a 192-atom supercell of Li_2O_2 (left). Each oxygen in the Li_2O_2 bonds with six Li^+ ions (right). (b) Schematic diagram of orbital energies of O_2^{2-} (left), elucidating the bonding nature of the electronic states of Li_2O_2. The filled and open circles represent, respectively, occupied and unoccupied electron states. The projected densities of states (PDOS) of Li_2O_2 were calculated using the HSE hybrid density functional (right). The valence band maximum is set to zero.

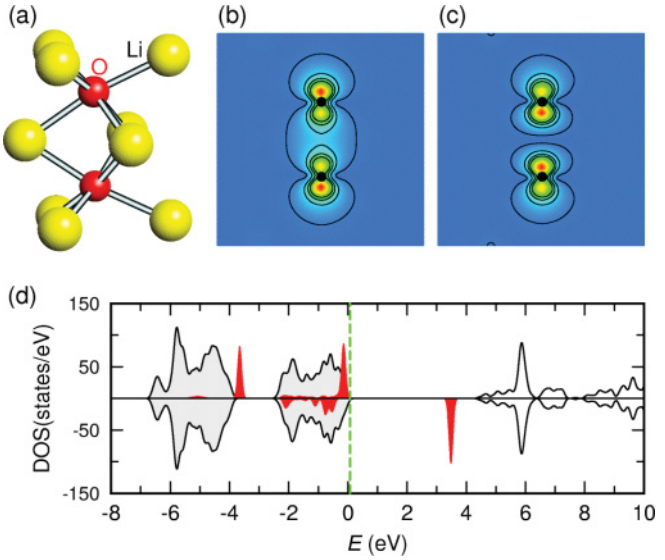

FIG. 2. (Color online) (a) The local atomic structure of a small polaron and (b)–(c) associated electronic states localized at the broken O–O bond. The positions of the oxygen atoms are denoted by dots. The interval between the contour lines is $0.1e$ Å^{-3}. (d) Total electronic density of states (DOS) of a 192-atom supercell containing a single polaron (black solid line) for majority (top) and minority (bottom) spin states. The valence band maximum is set to zero. The dark (red) shaded area is the spin-polarized, partial DOS projected on the local oxygen p_z orbitals of the cleaved O–O bond, which is enlarged by a factor of 30. The vertical dashed line denotes the Fermi energy.

III. RESULTS AND DISCUSSION

The structure of bulk Li_2O_2 contains an array of O_2^{2-} molecular ions that connect to a matrix of Li^+ ions [Fig. 1(a)]. The O–O bond length (d_{O-O}) is 1.51 Å. The electronic structure of Li_2O_2 stems from the electronic states of an isolated O_2 molecule in the 2- charge state with the two extra electrons donated by two Li atoms (forming Li^+). The chemical bonding of O_2^{2-} is understood by coupling two of the oxygen $2p$ orbitals [Fig. 1(b)]. The atomic arrangement of O_2 leads to an ordering sequence of the molecular orbitals of σ_p, π_p, π_p^*, and σ_p^*, and these orbital are occupied by 10 electrons [Fig. 1(b)]. The σ_s and σ_s^* orbitals that are occupied by four electrons are not shown. The fully occupied σ_p, π_p, and π_p^* orbitals comprise the valence bands of bulk Li_2O_2, whereas the empty, antibonding σ_p^* states, as well as the Li s states, provide the conduction bands, with a band gap of 4.5 eV in HSE. The HSE band gap is close to the GW band gap of 4.91 eV (Ref. 5). The Li s states lie above the σ_p^*-derived conduction states.

The molecular nature (σ_p^*) of the conduction band states leads to unique electron–lattice interaction in Li_2O_2, which makes a delocalized electron in the conduction band of Li_2O_2 unstable against formation of a small polaron. We found that the presence of an excess electron in Li_2O_2 results in elongation and/or cleavage of one of the O–O bonds (d_{O-O} = 2.2 Å) [Fig. 2(a)], and the excess electron is localized at the cleaved O–O site. Consequently, an occupied, localized, spin-up antibonding state of the elongated O–O bond appears near the valence band maximum, whereas a spin-down antibonding state inside the gap is not occupied [Figs. 2(c) and 2(d)]. This system thus has a magnetic moment of $\mu = 1\ \mu_B$. At the same time, a localized spin-up bonding state of the elongated O–O bond appears around −3.5 eV inside the π_p–π_p^* valence band gap [Figs. 2(b) and 2(d)], whereas the spin-down bonding state is resonant inside the top of the valence band. The self-trapping of the electron is due to the energy gain from the lowering of the occupied σ_p^* antibonding state and spin polarization. Our calculations show that this energy gain is much larger than the energy cost of the bond-breaking lattice distortion. Thus, the polaron state is 2.3 eV more stable than the case with an excess, delocalized electron in the conduction band of perfect Li_2O_2.

To check whether thermal or zero-point vibrations of light Li ions affect the stability of the polaron state, we compared two energy surfaces of Li_2O_2 with an excess electron in the small polaron state and in an extended electron state [Figs. 3(a) and 3(b)]. To model the phonon effect, the three equivalent Li ions around an O–O site were displaced from the equilibrium positions, while other atoms were fully relaxed. We found that the polaron state is always the ground state, regardless of the Li–Li distance (d_{Li-Li}). Despite the relatively small mass of Li ions, the zero-point energy was calculated to be only ∼30 meV. Thus, thermal or quantum vibrations of Li ions do not affect the stability of the small polaron.

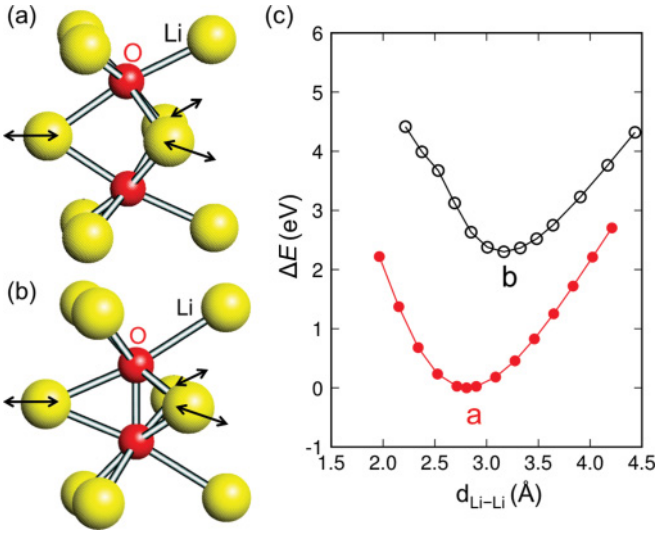

FIG. 3. (Color online) Comparison of total energies of Li_2O_2 with an excess electron at two electronic states as a function of d_{Li-Li}. (a) The excess electron is localized at the cleaved O–O site, forming a polaron state. (b) The electron is in an extended band state with energy equal to the conduction-band minimum energy of bulk Li_2O_2. (c) The corresponding energy curves are shown. ΔE is the relative energy with respect to the energy of the polaron state at its equilibrium geometry. The polaron state is always the ground state, regardless of d_{Li-Li}, indicating that thermal vibrations of Li ions do not affect the stability of the small polaron.

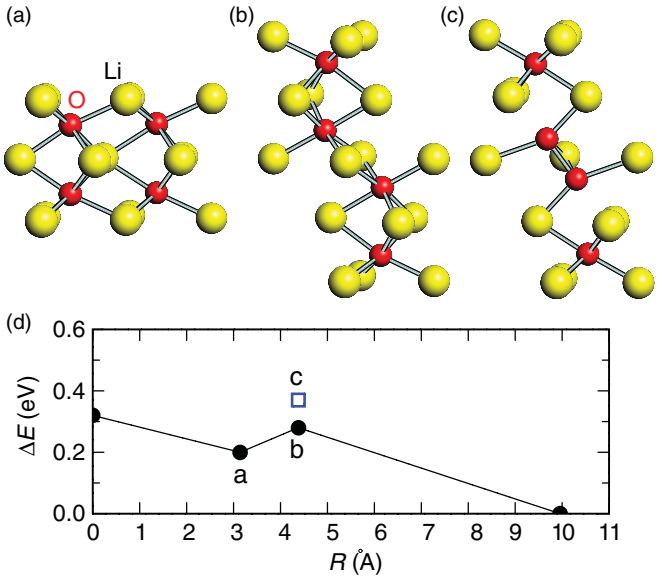

FIG. 4. (Color online) (a)–(c) Atomic structures of a pair of small polarons in bulk Li_2O_2. (d) Relative energies (ΔE) of the polaron pairs as a function of the polaron–polaron distances (R). The energy of the two well-separated polarons at $R = 10$ Å is set to zero. The result at $R = 0$ corresponds to the case in which an isolated polaron in Li_2O_2 traps two electrons.

The effect of the formation of small polarons in Li_2O_2 is similar to that of the DX^- center formation in AlGaAs and compressed GaAs,[23] which limits electron carrier density and mobility in n-type doped semiconductors. The DX^- defect involves a large displacement of an atom along a tetrahedral bond axis. Then, a deep and localized state is formed as a result of the bond-breaking lattice relaxation. The DX^- center is stabilized by two electrons occupying the localized state, while only one electron is needed to stabilize a small polaron in Li_2O_2 due to the large spin-exchange splitting of the O $2p$ orbitals and the weakened O–O bond of O_2^{2-} in the matrix of Li^+ ions.

Figure 4 shows the relative stability of two small polarons, each occupied with one electron, for different configurations and separation distances (R). For the polaron pair at the second nearest-neighbor distance ($R = 4.4$ Å), two configurations exist, as shown in Figs. 4(b) and 4(c). We also tested the case in which a broken O–O site of Li_2O_2 traps two electrons that becomes non-spin-polarized (i.e., $R = 0$). We found that the single polaron occupied by two electrons is 0.32 eV less stable than two well-separated polarons $R = 10$ Å, indicating the importance of the spin polarization in stabilizing the polarons in Li_2O_2. The energy of a polaron pair generally decreases with increasing R due to Coulomb repulsion. Therefore, the polarons are distributed uniformly in Li_2O_2, rather than forming bipolarons.

Next, we investigated the electron conduction mechanism in Li_2O_2. Electrons associated with small polarons are trapped by the broken O–O bonds. Thus, electron transfer subsequently requires successive bond cleaving and the reformation of O_2 from Li_2O_2. Hence, the migration of small polarons is a thermally activated hopping process. In general, polaronic mobility depends on the energy scales in play, such as phonon frequency, bare electron hopping, and electron–phonon coupling, as demonstrated by the model calculations[24–27] of the Holstein[24] and the Su-Schrieffer-Heeger[25] models.

For an accurate first-principles description of small polaron hopping, we need to employ a nonadiabatic approach in which electron evolution is described by a time-dependent Schrödinger-like equation. However, such a nonadiabatic approach is not currently available. Another approach to describing polaronic electron transfer is to employ the empirical Marcus model.[14] However, the key parameters of this model (i.e., the reorganization energy and the electron coupling) are difficult to calculate for solids.[11] Here, we assume an adiabatic electron transfer process for polaron hopping.[11,15] Using the nudged elastic band method,[28] we calculated the activation energy of the polaron migration. There are two paths for site-to-site hopping of polarons. In Fig. 5(a), interlayer hopping from site A to site B provides electron conduction with components in both the [001] and the [100] directions, while intralayer polaron hopping within the (001) plane (not shown here) allows polaron migration in only the [100] direction. The activation energy barriers (E_a) are calculated to be 0.54 and 0.66 eV for inter- and intralayer hopping, respectively. The transition state of each path has the same magnetic moment ($\mu = 1\ \mu_B$) with the initial and the final polaron states. For interlayer hopping, the change of electron charge distribution is shown in Figs. 5(a)–5(c). For the initial and final states, the electron is well localized on either site A or site B [Figs. 5(a) and 5(c)]. At the transition state, the electron is now shared by the two sites, with weak $pp\pi$-like bonding, as shown in Fig. 5(b). The $pp\pi^*$ antibonding state, which is empty,

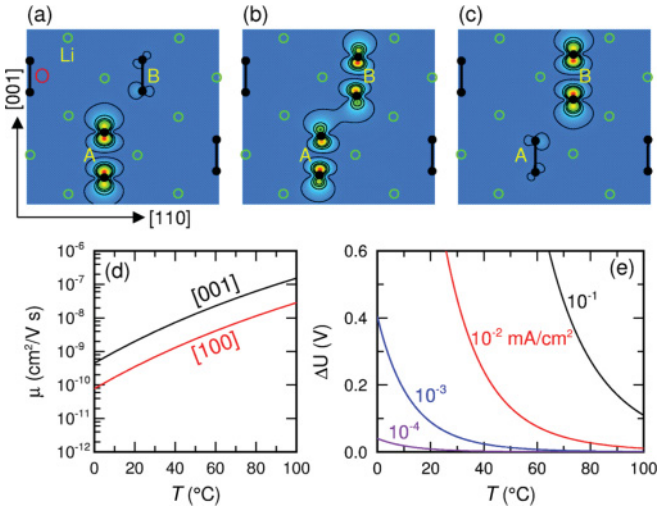

FIG. 5. (Color online) (a)–(c) The atomic structures and associated electron charge distributions plotted for interlayer hopping between site A and site B. The interval between the contour lines is $0.1e$ Å^{-3}. (d) The calculated electron mobility is plotted for [001] and [100] as a function of temperature. (e) The temperature dependence of the overpotential ΔU is shown for current densities ($J_{Li_2O_2}$) in the Li_2O_2 layer ranging from 10^{-4} to 10^{-1} mA/cm^2. Here, we fixed the layer thickness and the polaron density to $L = 50$ nm and $n = 10^{18}$ cm^{-3}, respectively.

lies at an energy that is higher than that of the occupied bonding state by 0.44 eV. The $pp\pi$ coupling lowers the E_a of interlayer hopping. In contrast, intralayer hopping within the (001) plane does not involve such electronic coupling between the hopping sites, leading to an E_a higher than that of interlayer hopping.

We also calculated the electron mobility (μ) in Li_2O_2 via small polaron hopping. The μ at temperature T is calculated from the Einstein relation[29] $\mu = eD/k_BT$, where k_B is the Boltzmann constant and D is the diffusion coefficient of small polarons, $D = Na^2\ \nu\ \exp(-E_a/k_BT)$. Here, N is the number of neighboring hopping sites ($N = 6$), and a is the distance between the hopping sites. The vibration frequency ν of O_2 in Li_2O_2 is $\sim 10^{13}$ Hz. The calculated μ for the [001] and [100] directions are shown in Fig. 5(d) as a function of T. Both the intra- and the interlayer hopping processes contribute to the electron mobility along [100], but interlayer hopping contributes more due to its lower activation energy. The calculated electron mobility is extremely low ($\mu = 10^{-10}$–10^{-9} cm^2/V s) at room temperature due to the nature of slow polaron hopping, with large thermal activation energy.

Finally, we discuss how the low electron mobility of Li_2O_2 affects the electrochemical reaction in the AC of LABs, i.e., $2Li^+ + 2e + O_2 \leftrightarrow Li_2O_2$. This cathode reaction requires electron transport from a substrate to a surface of Li_2O_2 during discharge. Here, we assumed that the formed Li_2O_2 provides the electron conduction path needed for the cathode reaction. The current density $J_{Li_2O_2}$ in a Li_2 O $_2$ particle is given by $J_{Li_2O_2} = \mu\ n\ e\ dU/dL$, where n is the number density of small polarons and e is the electric charge of an electron. U in the equation is the electric potential. L is the thickness of the Li_2O_2 layer, and it increases or decreases during discharge or charge, respectively. Because the (100) plane is the most stable Li_2O_2 surface,[5] we assumed that the [100] growth direction of Li_2O_2 is most applicable. The applied electric field inside the Li_2O_2 layer in the growth direction is given by $dU/dL \approx \Delta U/L$. Therefore, the voltage difference ΔU across the Li_2O_2 layer is estimated from $\Delta U = \frac{J_{Li_2O_2} L}{\mu n e}$. Figure 5(e) shows the calculated ΔU for different T and $J_{Li_2O_2} = 10^{-4}$–10^{-1} mA/cm^2 within the Li_2O_2 layer and assuming $L = 50$ nm and $n = 10^{18}$ cm^{-3}. $J_{Li_2O_2}$ is *different* from the *geometric* current density experimentally measured per unit area of the electrode.[30] The simulated overpotential ΔU becomes significant, more than 0.5 V at room temperature for $J_{Li_2O_2} > 0.01$ mA/cm^2, and it contributes in part to the large polarization of LABs. Hence, the low electron mobility limits the power density and efficiency of LABs. Due to the large anisotropy of μ [Fig. 5(d)], the overpotential ΔU depends on the growth direction of Li_2O_2. ΔU is an order of magnitude smaller for the [001] growth direction than for the [100] growth direction. We thus expect that the performance of LABs can be improved by selecting the optimal growth direction of Li_2O_2 on an appropriate substrate.

The low electron mobility of the small electron polarons is an intrinsic property of Li_2O_2. Hence, to significantly improve the performance of LABs at high current densities, we need alternative carrier conduction paths for the cathode reaction. Unlike electrons, the holes in Li_2O_2 do not form small polarons. This asymmetry between electron and hole arises from the different molecular nature of the conduction band state (σ_p^*) and the valence band state (π_p^*). Because the π bond is much weaker than the σ bond, the hole–lattice interaction associated with the valence band states is too weak to form a hole polaron state. So, we expect that p-type doping in Li_2O_2 could result in higher hole mobility and thus enhanced power density.

IV. CONCLUSIONS

We have shown that the self-trapping of electrons in the small polarons limits the electron mobility in Li_2O_2. An excess electron in the conduction band lowers its energy by cleaving an O–O bond of Li_2O_2 and forming a small polaron. The energy gain is caused by the lowering of the occupied σ_p^* orbital energy and the strong spin polarization of the O $2p$ state. The extremely low mobility, $\mu = 10^{-10}$–10^{-9} cm^2/V s, contributes to the substantial overpotential at high current density, which limits the power density of LABs. We suggest that designing alternative carrier conduction paths for the cathode reaction and/or p-type doping Li_2O_2 could result in dramatically improved performance. Thus, both further theoretical and further experimental efforts are required to test these predictions.

ACKNOWLEDGMENTS

We thank J. Yu for useful discussions. This work was funded by the National Renewable Energy Laboratory (NREL) Laboratory Directed Research and Development program (DE-AC36-08GO28308). The research employed the capabilities of NREL Computational Science Center (DE-AC36-08GO28308) and National Energy Research Scientific Computing Center (DE-AC02-05CH11231).

*joongoo.kang@nrel.gov

[1] M. Armand and J.-M. Tarascon, Nature **451**, 652 (2008).
[2] T. Ogasawara, A. Débart, M. Holzapfel, P. Novák, and P. G. Bruce, J. Am. Chem. Soc. **128**, 1390 (2006).
[3] A. Débart, A. J. Paterson, J. Bao, and P. G. Bruce, Angew. Chem. Int. Ed. **47**, 4521 (2008).
[4] G. Girishkumar, B. McCloskey, A. C. Luntz, S. Swanson, and W. Wilcke, J. Phys. Chem. Lett. **1**, 2193 (2010).
[5] J. S. Hummelshøj, J. Blomqvist, S. Datta, T. Vegge, J. Rossmeisl, K. S. Thygesen, A. C. Luntz, K. W. Jacobsen, and J. K. Nørskov, J. Chem. Phys. **132**, 071101 (2010).
[6] Y.-C. Lu, Z. Xu, H. A. Gasteiger, S. Chen, K. Hamad-Schifferli, and Y. Shao-Horn, J. Am. Chem. Soc. **132**, 12170 (2010).
[7] J. Hassoun, F. Croce, M. Armand, and B. Scrosati, Angew. Chem. Int. Ed. **50**, 2999 (2011).
[8] J. P. Zheng, R. Y. Liang, M. Hendrickson, and E. J. Plichta, J. Electrochem. Soc. **155**, A432 (2008).
[9] D. Emin and T. Holstein, Phys. Rev. Lett. **36**, 323 (1976).
[10] O. F. Schirmer, M. Imlau, C. Merschjann, and B. Schoke, J. Phys. Condens. Matter **21**, 123201 (2009).
[11] T. Maxisch, F. Zhou, and G. Ceder, Phys. Rev. B **73**, 104301 (2006).
[12] H. H. Nahm and C. H. Park, Phys. Rev. B **78**, 184108 (2008).
[13] S. Lenjer, O. F. Schirmer, H. Hesse, and Th. W. Kool, Phys. Rev. B **66**, 165106 (2002).
[14] R. A. Marcus, Rev. Mod. Phys. **65**, 599 (1993).
[15] D. Emin and T. Holstein, Ann. Phys. **53**, 439 (1969).
[16] O. F. Schirmer, J. Phys. Condens. Matter **23**, 334218 (2011).
[17] P. de la Mora and L. G. Cota, Acta Cystallogr. B **61**, 133 (2005).
[18] H. Y. Wu, H. Zhang, X. L. Cheng, and L. C. Cai, Phys. Lett. A **360**, 352 (2006).
[19] S. Heyd, G. E. Scuseria, and M. Ernzerhof, J. Chem. Phys. **118**, 8207 (2003).
[20] G. Kresse and J. Furthmüller, Phys. Rev. B **54**, 11169 (1996).
[21] J. P. Perdew, K. Burke, and M. Ernzerhof, Phys. Rev. Lett. **77**, 3865 (1996).
[22] P. E. Blöchl, Phys. Rev. B **50**, 17953 (1994).
[23] D. J. Chadi and K. J. Chang, Phys. Rev. Lett. **61**, 873 (1988).
[24] T. Holstein, Ann. Phys. **8**, 325 (1959); **8**, 343 (1959).
[25] W. P. Su, J. R. Schrieffer, and A. J. Heeger, Phys. Rev. Lett. **42**, 1698 (1979).
[26] I. Meccoli and M. Capone, Phys. Rev. B **63**, 014303 (2000).
[27] S. Fratini and S. Ciuchi, Phys. Rev. Lett. **91**, 256403 (2003).
[28] G. Mills, H. Jónsson, and G. K. Schenter, Surf. Sci. **324**, 305 (1995).
[29] A. Einstein, *Investigations on the Theory of the Brownian Movement* (Dover, New York, 1956).
[30] The amount of the large-surface-area carbon (LSAC) on the electrode is $\sim$10 mg/cm$^2_{(\text{electrode})}$, and the Brunauer-Emmett-Teller (BET) surface area of LSAC is $\sim$500 cm$^2_{(\text{BET})}$/mg. So, we estimate that 1 cm$^2_{(\text{electrode})} = 5000$ cm$^2_{(\text{BET})}$. The actual surface area on which Li_2O_2 particles grow would be much smaller than the BET area by a factor α of at least 100. Then, the geometric current density is estimated by $J_{\text{electrode}} = 5000\, J_{Li_2O_2}/\alpha = 50\, J_{Li_2O_2}$. For instance, a high current density of 25 mA/cm$^2_{(\text{electrode})}$, which is required for electric vehicles (Ref. 4), corresponds to $\sim$0.5 mA/cm$^2_{(Li_2O_2)}$.